Quiescent Signal Analysis for IC Diagnosis

James F. Plusquellic, Chintan Patel and Ying Ouyang

Department of Computer Science & Electrical Engineering
University of Maryland Baltimore County

Abstract

The use of I_{DDQ} test as a defect reliability screen has been widely used to improve device quality. However, the increase in subthreshold leakage currents in deep-submicron technologies has made it difficult to set an absolute pass/fail threshold. Recent work has focused on strategies that calibrate for process and/or technology-related variation effects. In this paper, a new I_{DDQ} technique is proposed that is based on an extension of a V_{DDT}-based method called Transient Signal Analysis (TSA). The method, called Quiescent Signal Analysis or QSA, uses the I_{DDQ}s measured at multiple supply pins as a means of localizing defects. Increases in I_{DDQ} due to a defect are regionalized by the resistive element of the supply grid. Therefore, each supply pin sources a unique fraction of the total I_{DDQ} drawn by the defect. The method analyzes the regional I_{DDQ}s and "triangulates" the position of the defect to an (x,y) location in the layout. This information can be used in combination with fault dictionary-based techniques as a means of further resolving the defect's location.

1.0 Introduction

I_{DDQ} has been used extensively as a reliability screen for shorting defects in digital integrated circuits. Unfortunately, traditional I_{DDQ} methods applied to devices fabricated in newer deep-submicron technologies are resulting in unacceptably high levels of yield loss. The significant increase in subthreshold leakage currents in these technologies is making it difficult to set an absolute pass/fail threshold that fails only defective devices [1]. Several methods have been proposed as solutions to the subthreshold leakage current problem and, more recently, to process variation issues. Current signatures [2], delta-I_{DDQ} [3] and ratio-I_{DDQ} [4] are based on a "self-relative" analysis, in which the "average" parametric behavior of each device is factored into the pass/fail threshold value. In the following discussion, we will refer to the technology dependency of subthreshold leakage current as a *technology-related variation* effect to contrast it with the chip-to-chip variation effects caused by changes in process parameters (*process variation*).

The approach proposed in this paper is based on a previous V_{DDT}-based method called Transient Signal Analysis (TSA) [5]. TSA uses regression analysis to calibrate for process and technology-related variation effects by cross-correlating multiple supply pin transient signals measured under each test sequence. The I_{DDQ} method proposed in this paper, called Quiescent Signal Analysis or QSA, uses a set of I_{DDQ} measurements instead, each obtained from the individual supply pins of the Device-Under-Test (DUT). The process and technology calibration procedure used in QSA is based on a regression analysis procedure similar to TSA.

In TSA, we referred to signal variation resulting from defects as regional variation, to contrast it with the global variations introduced by process and technology-related effects. For transient signals, the supply rail's impedance network modifies signal characteristics, such as phase and magnitude, at different supply pin test points. In QSA, only the resistive component of the supply rail network introduces variation in the I_{DDQ} values at different supply pins. In either case, the position of the defect in the layout with respect to any given power supply pin is related to the amount of regional "defect" variation observed at that pin. For QSA, the variation is directly related to the resistance between the defect site and the pin. For example, a larger value of I_{DDQ} is expected on supply pins closer to the defect site because of the smaller R. Therefore, the multiple I_{DDQ} measurements can be used to detect the defect as well as "triangulate" the physical position of the defect in the layout.

Defect detection experiments are on-going and will be addressed in a future work. In this work, a diagnostic method for QSA is developed and a set of simulation results are presented to demonstrate its defect localization accuracy. A characterization procedure is proposed that can be performed beforehand to determine the mapping between resistance and distance in the layout. Our results show that the (x,y) prediction given by the method is within 10% of the actual defect location. This suggests that the technique is best used in combination with fault dictionary techniques as a means of further resolving the defect's location.

This paper is organized as follows. Section 2.0 describes related work. Section 3.0 presents the experimental design. Section 4.0 describes the method. Section 5.0 presents the results of experiments. Section 6.0 discusses

the regression analysis technique that can be used to calibrate for process variation effects. Section 7.0 provides a summary and conclusions.

2.0 Background

Several diagnostic methods have been developed based on I_{DDQ} measurements. In general, these methods produce a list of candidate faults from a set of observed tester failures using a fault dictionary. The likelihood of each candidate fault can be determined by several statistical algorithms. For example, signature analysis uses the Dempster-Shafer theory, which is based on Bayesian statistics of subjective probability [9]. Delta I_{DDQ} makes use of the concepts of differential current probabilistic signatures and maximum likelihood estimation [10]. Although these methods are designed to improve the selection of fault candidates, in many cases, they are not able to generate a single candidate. Other difficulties of these methods include the effort involved in building the fault dictionary and the time required to generate the fault candidates from the large fault dictionary using device tester data.

The QSA procedure proposed here can help in the selection of the most likely candidate from the candidate list produced by these algorithms. The physical layout information generated by our method can be used with information that maps the logical faults in the candidate lists to devices in the layout. In addition, it may be possible to use the (x,y) location information provided by QSA as a means of reducing the search space for likely candidates in the original fault dictionary procedure. This can reduce the processing time and space requirements significantly.

3.0 Experimental Design

QSA experiments were conducted on a full-custom design of an 8-bit 2's complement multiplier. A block diagram of this device is shown in Figure 1. The primary inputs, labeled A[0] through A[7] and B[0] through B[7] are shown along the top and right of the figure. Only ten of the primary outputs are wired to the pad frame (and observable at the package pins of the device.) The power supplies for the core logic are labeled as V_{DD1} through V_{DD8} and are distributed evenly along the periphery of the core logic. The core logic consists of a rectangular array of AND gates and full adders, shown as squares in the center of the figure. Bridging and open defects were inserted into these cells at the approximate locations shown by the Xs in the figure. The SPACE extraction tool was used to generate RC models from the layout [11].

Two methods are used to measure the individual I_{DDQ} values at the supply pads shown in Figure 1. In a SPICE simulation environment, the most straightforward method is to use the V_{DD} branch currents of the ideal sources directly. For production test, this corresponds to using the

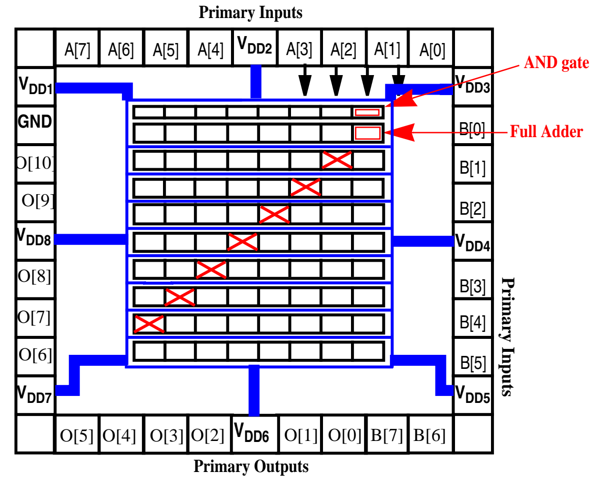

Figure 1. The layout of the 8-bit multiplier.

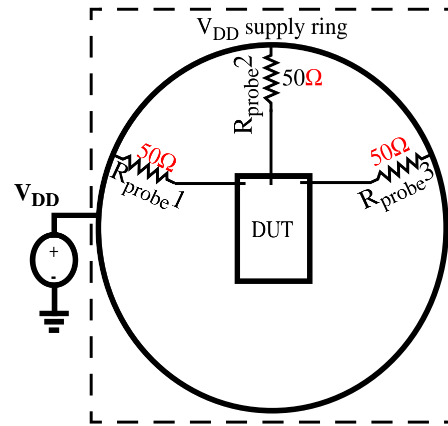

Figure 2. Probe card model.

tester electronics at wafer probe to monitor a set of power supplies that drive each of the V_{DD} pads. It is recognized that this may not be possible due to tester limitations on available power supply channels. Therefore, a second method based on voltage measurements is proposed. At wafer probe, it is possible to measure the current as a voltage drop by inserting series resistors between the supply pads and the supply ring on the probe card, as shown in Figure 2. The value of the series resistance (50 Ohms in our experiments) depends on the "average" steady-state current drawn by devices in the process. It may be necessary to "switch out" the resistors to prevent excessive supply rail voltage drops, when the DUT is switched between states.

4.0 Experimental Method

In this section, we describe the QSA technique used for localizing shorting defects. Since the simulations were carried out on circuit models derived from a 2.0um nwell technology, background current were very small (~30nA) and, therefore, are not accounted for directly in this section. However, Section 6.0 describes several extensions of the

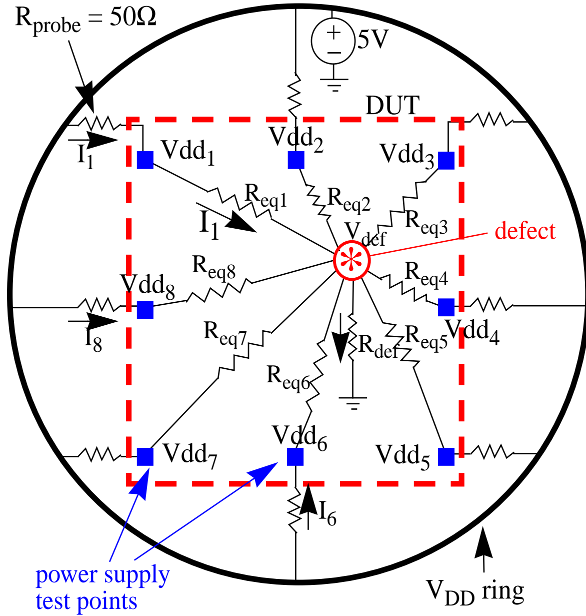

Figure 3. Equivalent resistance network with defect inside the circuit.

method that "calibrate" for the significant leakage currents associated with current technologies.

The method is composed of two phases: Resistance Network Analysis and Resistance-to-Distance Analysis.

- Phase 1: Resistance Network Analysis

The objective of this phase is to determine the "equivalent resistance" (R_{eq}s) between each of the supply pads and the point from which the defect draws current from the supply grid. The R_{eq}s are labeled R_{eq1} through R_{eq8} in Figure 3. The R_{eq}s are computed by setting the state of the circuit such that the short is provoked and the voltages at each of the supply pads is measured. Under this condition, the defect will draw current from each of the supply pads proportional to the value of the R_{eq}. As explained in the previous section, the 50 Ohm resistor (R_{probe}) placed in series with the supply pad probes allows the currents to be measured as voltage drops in these experiments. If the appropriate measurement instrumentation is available, I_1 through I_8 can be obtained directly.

Figure 4 shows the supply pad voltages from a simulation of a device with a defect inserted at the location shown in Figure 3. The steady-state values shown along the left portion in the figure indicate that the defect causes a regional current variation in the device. The ordering of the voltage waveforms (from top to bottom) in Figure 4 is inversely related to the R_{eq}s between the supply pads and the defect site. Therefore, the supply pads with the largest voltage drops indicate they are in close proximity to the defect. Although it is unlikely that the relationship between

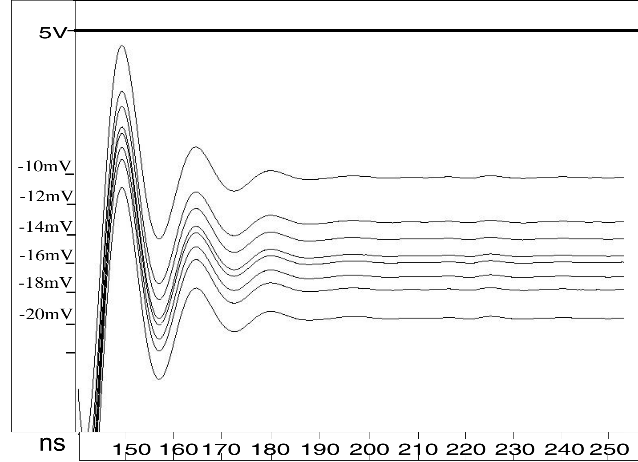

Figure 4. Voltage waveforms measured at the eight supply pins with the shorting defect provoked.

R and distance is strictly linear and uniform along all directions from the supply pads to points in the layout, it is certainly valid to assume it approaches such a function if the supply topology is grid-like and regular. We will show that good results are obtained under this assumption for our experimental circuit. A procedure for dealing with irregular topologies is proposed in the next section.

Since the I_{DDQ} values are related only to the resistive components of the network as shown in Figure 3, the following system of equations can be written to describe its behavior. The I_i variable represents the branch currents

$$I_i \times (R_{eqi} + R_{probe}) = V_{def} \text{ for i = 1 ... 8}$$
$$\text{i = 1 ... 8}$$

Equation 1. System of equations

through each of the supply pins, R_{probe} is known (50 Ohms in our experiments), and R_{eqi}s are the unknowns. The voltage at the defect site (V_{def} at the "star" in the figure) is also unknown but can be used as the point of reference for the system of equations. This formulation yields 8 equations and 9 unknowns. Therefore, without additional information, we cannot solve for the R_{eqi}s. However, the important information is the *relative differences* between the R_{eqi}s and not their absolute values. This relationship is captured by computing ratios. As described in the next section, the ratios can be scaled as easily as the real Rs to obtain the location of the defect. The ratios of the resistances R_{eq1} to R_{eq8} are computed from the equations given in Equation 2 below.

These equations express 7 of the R_{eqi}s as a function of the 8th. Any R_{eqk} can be chosen as the reference resistance.

- Phase 2: Resistance-to-Distance Analysis

The objective of this phase is to map from the equiva-

$$I_i \times (R_i + R_{probe}) = I_k \times (R_k + R_{probe})$$

$$R_i = \frac{I_k}{I_i} \times R_k + \left(\frac{I_k}{I_i} - 1\right) \times R_{probe}$$

for i = 1 ... 8 excluding k

Equation 2. Resistance ratios of R_1 to R_8

lent R_{eq}s to a set of distances in the layout, each directed from a supply pad to the defect site. In the ideal case, the resistances scale linearly to distance uniformly along any vector. However, complex and/or irregular supply topologies routed in multiple levels of metal with resistive contacts connecting them, can complicate the resistance to distance mapping function. Two mapping functions are described; one the assumes linearity and a second that handles more complex functions.

i) Method 1:

This method simply uses the resistance ratios as distance ratios, which are scaled by a common factor as a means of finding a point of intersection among them. The following steps summarize the process and its heuristics:

Step 1 Select the V_{DD} supply pad, V_{DDk}, closest to the defect site. This is equivalent to selecting the largest current value, I_k or the minimum resistance, R_{eqk} in Equation 2. Since d_k is assumed proportional to R_{eqk}, V_{DDk} is closest and is referred to as the primary supply pad.

Step 2 Select the supply pads with the second and third largest current values. These pads are likely neighbors of the primary supply pad. If the supply pad configuration is similar to the one shown in Figure 1, it is possible that these choices result in a line of pads along one dimension of the layout. For example, if the supply pads V_{DD3}, V_{DD4} and V_{DD5} are selected in the design shown in Figure 1, only the y dimension is "covered". In this case, the supply pad that ranks fourth in the sorted list of supply currents should be selected instead (e.g. V_{DD2}) since it "covers" the x dimension. Similar heuristics can be used for other supply pad configurations.

Step 3 Using the three selected supply pads, establish a set of circles with radii proportional to the ratios computed in Equation 2. The simple algorithm is used to iteratively scale the radii by the same factor and tests for intersection. The point of intersection indicates the (x,y) location in the layout at which the defect draws current from the supply grid.

An application of this method is shown in Figure 5 for Bridging Experiment #1. The figure represents the layout of the multiplier with the x and y scales given in units of lambda. The supply pad locations are shown as "stars"

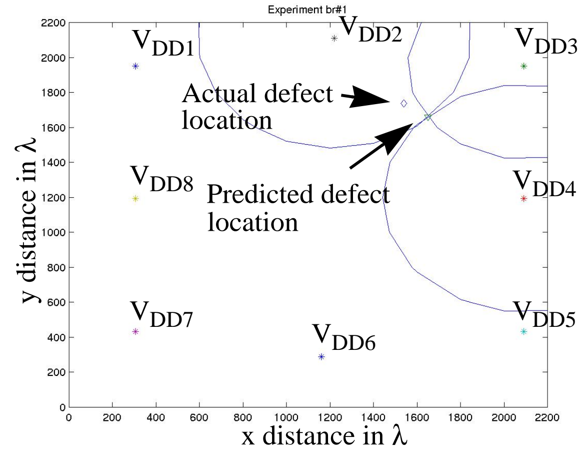

Figure 5. Bridging Experiment #1 using localization Method 1.

along the edges of the figure. Three circles are shown in the upper right hand corner centered around the supply pads V_{DD2}, V_{DD3} and V_{DD4}. These supply pads were selected because they sourced the largest currents, as given in Steps 1 and 2 in the method. The circles have been scaled so that they have a common point of intersection. The predicted and actual (x,y) locations are given by "star"s in the figure.

ii) Method 2:

The second method uses a contour to map resistance to distance in the layout. Since the actual mapping function is not easily obtained, this estimate is designed to provide a more accurate prediction for supply grid designs with irregular topologies. The data to construct the contour can be obtained easily using a defect-free device or a simulation model.

The method uses the equivalent R_{eq}s between the supply pads. They can be obtained between each pairing of supply pads by setting the supply pad under test to a voltage slightly less (e.g. 100mV) than the nominal supply voltage. The remaining supply pads are set to their nominal voltage and the currents measured. The distance between each pairing of supply pads is easily obtained from the layout. The ratio of distance and resistance defines the scaling factor along each of the vectored directions from the supply pad under test to the other supply pads. The experiments produce a set of contours (one for each supply pad) that are used instead of the circles in the localization procedure described for Method 1.

This method simulates the presence of a defect at each of the supply pads. Therefore, the R_{eq} obtained from the measurement accurately reflects the R for defects in the vicinity of that supply pad. The drawback of contours is that they may produce several different points of intersection under different scaling factors. Therefore, several predicted locations may be generated by the algorithm

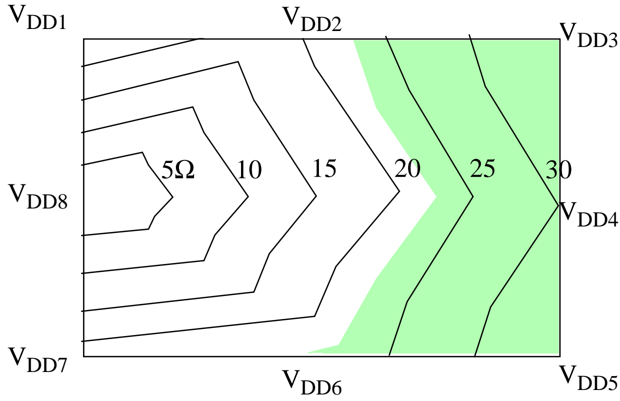

Figure 6. The resistance-to-distance mapping contour for V_{DD1}.

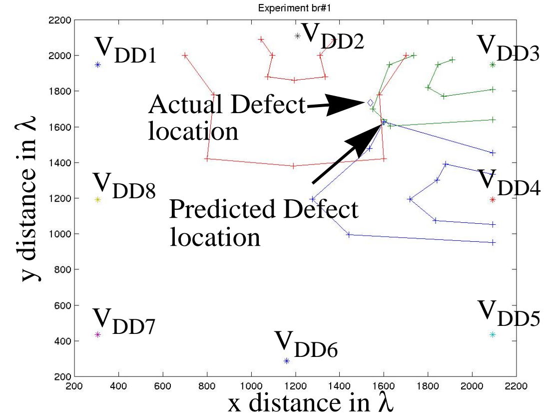

Figure 7. Bridging Experiment #1 localization using contour maps (Method 2).

described in Method 1 above.

Figure 6 shows the contour obtained for V_{DD1} in our experiments. The lines representing the contour are each labeled with the R_{eq} they define at points in the layout under their curve. A full set of contours would consist of one such mapping for each supply pin. Figure 7 shows the method applied to the resistance data obtained for Bridging Experiment #1. In comparison to the localization result shown in Figure 5, only slightly better results are obtained for this experiment using contour maps.

5.0 Experiments Results

The results of several experiments are shown using graphical representations in this section. A table is presented at the end of the section that summarizes the errors between the actual and predicted locations of the defects. The error is computed as the ratio of the distance between the predicted and actual (x,y) locations and the width of the layout. The localization curves for Bridging Experiment #1 are shown in Figures 5 and 7 and described in the previous section. The error for this experiment is approximately 7% using either Resistance-to-Distance Method 1 or 2.

Figure 8 shows a portion of the transmission-gate full adder schematic used in the design. The implementation uses a 2-to-1 MUX whose select lines are driven by an XOR gate and an inverter. The open is shown at the output of the inverter. The undriven node floats to 0V leaving the p-channel transistor in the upper transmission gate permanently on. Under a circuit state that causes the XOR to output a 0, the opposing values on the inputs to the MUX create a short as shown by the thick line in the figure. Figure 9 shows the results from this experiment in graphical form. The actual and predicted locations are indicated in the figure using supply pad test points V_{DD6}, V_{DD7} and V_{DD8}.

A summary of the prediction errors for the experiments is given in Table 1. The left-most column identifies

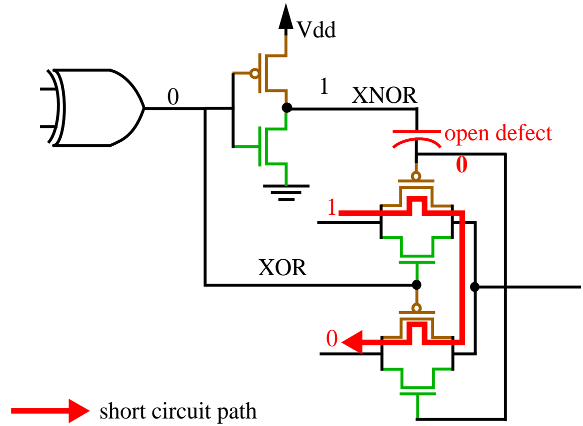

Figure 8. A portion of the transmission gate full adder illustrating the shorting behavior caused by an open defect.

the experiment. The second column gives the actual position of the defect in the layout (in units of lambda) and the third column gives the predicted location. The last column gives the error as described previously. The width of the layout is 2,200 lambda. As observed in the right-most column of the table, the worst case prediction result is less than 10%.

6.0 Process Variation and Leakage Current

The background leakage currents measured in the simulation experiments (< 30nA) were very small. However, in deep-submicron technologies, these currents are orders of magnitude higher and must be accounted for in any useful testing technique based on steady-state currents. Current signatures, delta-I_{DDQ} and ratio I_{DDQ} methods are proposed as alternatives. In this section, we describe a regression analysis procedure for QSA that can be used to calibrate for background currents. The method is adapted from the procedure defined for TSA (see [5]).

The defective device I_{DDQ} consists of two compo-

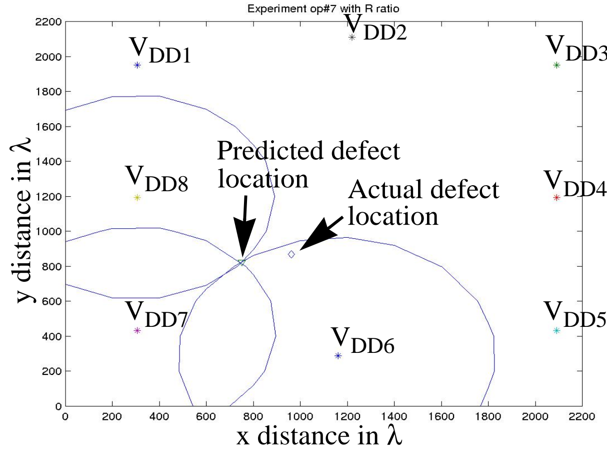

Figure 9. Open Experiment #7 results using localization Method 1.

nents, the current drawn by the defect, and the process and technology-related leakage current, e.g. subthreshold leakage current. This changes the formulation presented in Equation 2 to that shown in Equation 3 below.

$$(I_{leakagei} + I_{defecti}) \cdot (R_{eqi} + R_{probe})$$
$$= (I_{leakagek} + I_{defectk}) \cdot (R_{eqk} + R_{probe})$$

Equation 3. Equation 2 reformulated with background current

The leakage current is given as a set of currents, $I_{leakagei}$ in the equations, each representing the current drawn through each of the supply pins. If the transistor density in the layout is regular, then the leakage current will be evenly distributed among the supply pins yielding a single value for $I_{leakagei}$. However, if the transistor density in the layout varies across the design, then the $I_{leakagei}$ will also vary since the supply rail will distribute the current proportionally as a function of its resistance. The “localized” variation of the leakage current will adversely affect the localization methods described in the previous section unless it is accounted for.

The key observation concerning leakage current is that it is effected most significantly by the “global” variations introduced by changes in process and technology-related parameters. In other words, the current variations introduced by variations in these parameters will affect all transistors and junctions in a device in a similar manner. We are not claiming that intra-device variations do not exist, but rather that they are smaller in magnitude and can be ignored. The more significant global variations will scale the leakage currents in all supply rails proportionally, making it possible to track it using regression analysis.

A graphical representation of leakage current tracking behavior is shown in Figure 10. The x axis plots I_{DDQ} for supply pin k while the y axis plots it for supply pin i. The labeled points A through F represent measured values on these two pins from a set of defect-free devices. As noted in the figure, the pairs of I_{DDQ}s from each device track each other, e.g., changes in one value are matched by changes in the other value. The correlation in these pairings is tracked by the regression line (best fit line) shown in the figure. Unmodeled factors such as intra-device process variation and noise will make these data points non-colinear. Therefore, 3 sigma prediction limits are used to delimit a region around the line (labeled Process Variation Zone). It is within this region that the data points from defect-free devices are expected to fall.

In contrast, the “regional” variation caused by an

Table 1: Experiment results

Defect	Actual Location	Predicted Location	% Error
BR#1	(1540,1736)	(1640,1640)	6.3%
BR#2	(962,870)	(755,825)	9.5%
BR#3	(1465,1365)	(1580,1550)	9.9%
BR#4	(1460,1600)	(1600,1630)	6.5%
BR#5	(1120,1240)	(1173,1215)	2.6%
BR#6	(1020,1120)	(1150,1210)	7.1%
BR#7	(912,993)	(770,835)	9.5%
BR#8	(1064,950)	(1190,1209)	6.3%
OP#3	(1465,1365)	(1580,1550)	9.9%
OP#7	(962,870)	(760,835)	9.3%
OP#9	(880,830)	(735,800)	6.7%

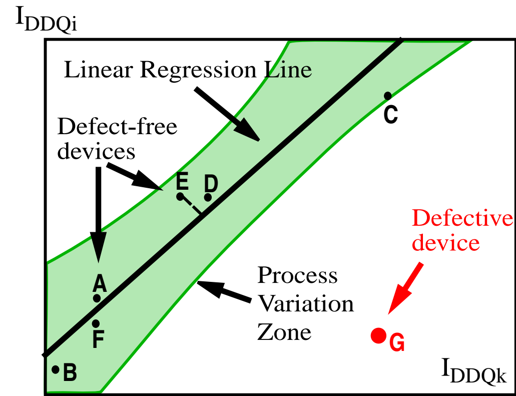

Figure 10. Scatter plot to determine the ratios between each two test points in defect free devices

active shorting defect will disrupt the correlation between the I_{DDQ}s from this pair of supply pins. The data point represented by G in the figure shows this graphically. Although we do not present results in this paper, defect detection is possible using a strategy based on the analysis of outliers (point G in the figure). The details of such a method are given in reference [5]. Since the focus of this paper is on diagnostics, only the procedure used to calibrate for process and technology variation effects is outlined here.

Figure 11 illustrates the "regional" versus "global" effect graphically. As indicated above, the background currents for our experiments are extremely small (<30nA). However, they are measurable in the noise free environment of the simulation. The waveforms shown in the figure represent the I_{DDQ}s under two different state vectors. The region labeled "Shorting Region" are the I_{DDQ}s when the circuit state is set such that the shorting defect is activated. The region on the right are the I_{DDQ}s measured under a non-shorting circuit state. Although it is not discernible in the figure, the ordering of I_{DDQ}s under the non-shorting circuit state is different than the ordering under the shorting state. The ordering is given in the figure. This is expected since the shorting condition adds different amounts of regional current to the background values depending on the location of the defect with respect to the supply pin. In contrast, the waveforms in either region from a defect-free device whose process parameters are different is expected to generate the same ordering in both regions as the ordering shown on the right in Figure 11.

From Equation 3, it is clear that the system of equations is solvable (in the fashion described in Section 4.0) if the $I_{leakagei}$s are known quantities. There are several alternatives for deriving these values, all of which depend on the existence of a set of scatterplots that correlate the expected I_{DDQ} values between the supply pins of the design. If it is true that the vector-to-vector background current variation remains correlated between the supply pins to a reasonable extent, then the regression analysis proposed above under a single state vector can be used across vectors. In this case, an accurate estimate of the $I_{leakagei}$s under the shorting circuit state can be obtained from measurements made from the same device under a non-shorting state. A second alternative involves computing the mean value from the set of defect-free characterization devices used to derive the scatterplots. If the vector-to-vector variation is small compared to process variation, then the mean value may be good estimates of the $I_{leakagei}$s.

The best alternative is to keep the vector-to-vector variation out of the picture. In other words, the best approach is to measure the I_{DDQ}s of the defective device

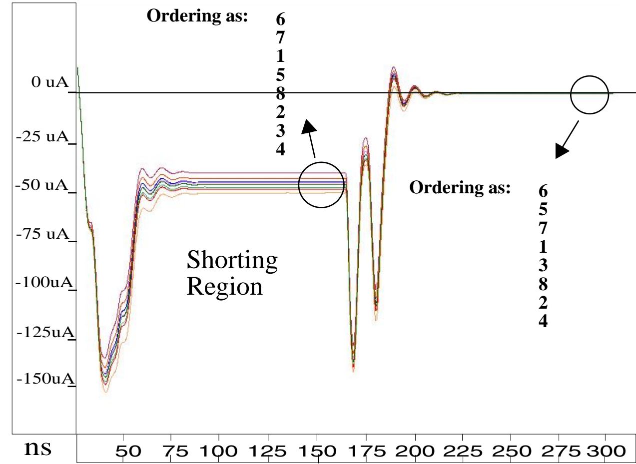

Figure 11. V_{DD} waveforms showing the effects of a shorting defect on the ordering of I_{DDQ} supply pin values

under the state vector that causes the short but to do so without causing the short. This is clearly impossible but an close approximation may be possible. The results presented previously give a total ordering of the I_{DDQs} under the shorted circuit state. The largest three current values were selected for the localization methods and the smaller values were ignored, since their supply pins were presumably further removed from the defect site. This suggests that the smallest of these values has the smallest fraction of current drawn by the defect. If it is assumed that this current is entirely leakage current, then this value can be used in a backward mapping across the scatterplots to obtain the fraction of total current that is leakage in each of the other supply pins. The $I_{leakagei}$s obtained can then be plugged into the equations given in Equation 3 and solved in a manner similar to that proposed for Equation 2.

7.0 Summary and Conclusions

In the paper, we describe a method based on the analysis of multiple power supply pin I_{DDQ} values for the localization of defects. The technique, which is called Quiescent Signal Analysis (QSA), consists of two phases. In the first phase, the relative values of the individual supply pin I_{DDQ}s are used as a means of determining the "equivalent" resistance between each supply pin and the defect site. In the second phase, a mapping function that relates resistances to positions in the layout is used to predict the location of the defect. The procedure is proposed for calibrating for leakage current due to process and technology-related variation effects that is based on linear regression analysis.

A set of simulation experiments were conducted on defective versions of an 8-bit multiplier circuit to demonstrate the method and its accuracy. The results of the experiments show that it is possible to predict the actual location

of the defect with less that 10% error. Although better results are expected as the accuracy of the extracted model is improved, this technique is best used in combination with fault dictionary-based techniques as a means of further resolving the defect's location.

With respect to a hardware implementation of the technique, our main concerns is related to instrumentation accuracy. The simulation results of the device in 2.0um technology indicate that the ratio between the resistance of the defect network to ground to the "equivalent" resistances (from the supply pin to the defect site) are on the order of 200 to 1. In other words, a defect that draws 1mA current will produce I_{DDQ} variations in each supply pin in the 10's of uA range. If the measurement instrumentation is capable of distinguishing between values in that range, then good defect localization accuracy is expected. Technology trends and a better extraction procedure may reduce this ratio in more advanced technologies, further improving the accuracy of the method.

Simulations and hardware experiments are underway to investigate other aspects of the QSA procedure. Among these include experiments designed to test the process calibration techniques proposed in section 6.0. The defect detection capabilities of the method will be evaluated in the course of the research.

References

[1] T.W.Williams, R.H.Dennard, R.Kapur, M.R.Mercer & W.Maly, "I_{DDQ} test: Sensitivity Analysis of Scaling", In proceedings *International Test Conference* 1996, pp.786-792.

[2] A.E.Gattiker and W.Maly, "Current Signatures", In proceeding *VLSI Test Symposium*, 1996, pp.112-117.

[3] C. Thibeault, "On the Comparison of Delta I_{DDQ} and I_{DDQ} test", In proceedings *17th IEEE VLSI Test Symposium*, 1999, pp. 143-150.

[4] Peter Maxwell, Pete O'Neill, Rob Aitken, Roland Dudley, Neal Jaarsma, Minh Quach, Don Wiseman, "Current Ratios: A self-Scaling Technique for Production IDDQ Testing", In proceedings *International Test Conference*, 1999, pp.738-746.

[5] Amy Germida, Zheng Yan, J. F. Plusquellic and Fidel Muradali. "Defect Detection using Power Supply Transient Signal Analysis," In proceedings *International Test Conference*, 1999, pp. 67-76.

[6] T.M.Storey and W.Maly, "CMOS Bridging Fault Detection", In proceedings *International Test Conference*, 1991, pp.1123-1132.

[7] E.McCluskey(Moderator), K.Baker(Organizer), W.Maly, W.Needham, M.Sachdev(Panelists), "Will I_{DDQ} Testing Leak Away in Deep Sub-micron Technology?", *International Test Conference,* 1996, Panel 7.

[8] A.E.Gattiker and W.Maly, "Current Signatures for Production Testing", In proceedings *International Workshop on IDDQ Testing*, 1996, pp.25-281.

[9] Christopher L.Henderson and Jerry M.Soden, "Signature Analysis for IC Diagnosis and Failure Analysis", In proceedings *International Test Conference*, 1997, pp.310-318.

[10] C. Thibeault, L. Boisvert, "Diagnosis method based on delta I_{DDQ} probabilistic signatures: Experimental results", In proceedings *International Test Conference,* 1998, pp.1019-1026.

[11] Arjan van Genderen, Nick van der Meijs, Frederik Beeftink, Peter Elias, Ulrich Geigenmuller and Theo Smedes, Delft University of Technology, "SPACE, Layout to Circuit Extraction software module of the Nelsis IC Design System", (http://cas.et.tudelft.nl/~space/space_man.html).